

# ASTEROID'S ORBIT AND ROTATIONAL CONTROL USING LASER ABLATION: TOWARDS HIGH FIDELITY MODELLING OF A DEFLECTION MISSION

Massimo Vetrisano<sup>(1)</sup>, Nicolas Thiry<sup>(2)</sup>, Chiara Tardioli<sup>(2)</sup>, Juan L. Cano<sup>(1)</sup> and Massimiliano Vasile<sup>(2)</sup>

<sup>(1)</sup>Deimos Space S.L.U., Ronda de Poniente, 19, 28760 Tres Cantos, Madrid, Spain, +34 918063450, {massimo.vetrisano, juan-luis.cano}@deimos-space.com

<sup>(2)</sup>Department of Mechanical & Aerospace Engineering, University of Strathclyde, James Weir Building, 75 Montrose Street, University of Strathclyde, Glasgow | G1 1XJ | t:0141 548 2326, {nicolas.thiry, chiara.tardioli, massimiliano.vasile}@strath.ac.uk

**Abstract:** *This article presents an advanced analysis of a deflection mission considering the coupled orbit and attitude dynamics of an asteroid deviation mission through laser ablation. A laser beam is focused on the surface of an asteroid to induce sublimation. The resulting thrust induced by the jet of gas and debris from the asteroid, directed as the local normal to the surface, is employed to contactless manipulate its orbit. Based on the theoretical model of a laser-based deflector, an optimal hovering distance for the spacecraft operations and required power are first computed. A stability analysis of the orbit evolution for big size ejecta is also considered in order to place the spacecraft on relatively safe and debris free trajectory at the asteroid, assuming an impactor has been employed before the spacecraft arrival. Three operational control strategies are then analysed based on the laser system capabilities. Results show that it is not possible to significantly decrease the angular velocity of 100 m asteroid using relatively low power lasers during short period operation, nonetheless different options allow safely deflecting the asteroid orbit by one Earth radius.*

**Keywords:** *Asteroid's debris, asteroid deflection, asteroid attitude control, laser ablation.*

## 1. Introduction

Near Earth objects have been generating growing scientific interest because, as primordial remnants of our solar system, they preserve precious information about its formation, composition and evolution; besides, their collision with the early Earth, would have influenced the shape and composition of our planet. Some NEOs are especially attractive targets for low-cost missions, because of their orbital accessibility with current technologies and short flight duration. Nevertheless, NEO collision with the Earth represents a possible risk. A short-term threat is posed by a large number of small asteroids, which could cause local devastating effects to our planet. On the other hand, impact hazards with global catastrophic consequences could occur, on a long-term, if a larger kilometre-sized body were to hit the Earth ([1]). Advances in orbit determination and theoretical studies on hazard characterisation have increased the capability of predicting potential impacts. Increasing our capabilities in asteroid orbit and attitude manipulation is therefore a priority, both for protection of collision hazard and for future asteroid exploitation.

Currently there is a wide interest in a scientific demo to deflect a small asteroid [2]. In order to extend the scientific outcomes from missions to minor bodies, often an impactor is envisaged either to impart a small impulse or to eject materials and make it possible for a fellow spacecraft to identify the asteroid composition. In the case of a deflection, the kinetic impactor spacecraft is expendable. Either to measure the resulting deflection or to impart an additional velocity variation by means of low-push systems, a second probe would be required. Nonetheless the

cloud of debris produced by the previous impact could still pose a potential threat to these operations. For this reason, this paper studies the evolution of the ejected particles, the region where they orbit and the time the orbit can be considered clear of most hazards. It also true that the majority of debris will in general escape the weak gravity field after the impact. In fact we assumed a 100 m rotating asteroid using actual surface data to simulate the gravity field. In particular we focused our analyses only on particles with initial energy content below zero (i.e. not parabolic or hyperbolic) for different value of area to mass ratios and asteroid's angular velocity similarly to [3] where the asteroid was in the range of kilometres and the gravity field approximated to a second order ellipsoidal one.

Once the orbit is relatively safe we consider the asteroid is deflected through surface ablation which was shown to be theoretically one of the most promising methods [4]. The ablated material then expands to form an ejecta plume. The resulting thrust induced by the ejecta plume pushes the asteroid away from its original trajectory. This paper aims at improving available models used for asteroid deflection. Previous works [5][6] have considered small rocky asteroid and made simplifying assumptions regarding laser ablation process, asteroid's shape and dynamics. This paper integrates a refined finite volume laser model (FVM) derived in [7] which considers three-dimensional effects on the irregular facets of the asteroid.

This paper presents three different deflection strategies: 1) the laser is pointed on the surface points such to control the rotational motion of an asteroid similarly to the work of [6]; 2) the laser hits the surface points which produce a thrust as much as possible aligned to the tangential direction; 3) the laser pointing is maintained fixed. For practical reason the available power at the laser will be limited to 20 kW (at 1AU) at the beginning of the simulation (roughly 64 m<sup>2</sup> for the spacecraft Rosetta). The deflection of the asteroid over the pushing time with respect to its nominal orbit is computed through a semi-analytical approach. It will be shown that the second strategy is the most effective in achieving one Earth radius deflection, although as operationally complicated as the first. The final yield of the third indeed is comparable to the best option, while not requiring continuous pointing of the laser system.

This paper is organised as follows. Section 2 introduces the dynamics model for the debris leaving the surface of the asteroid. Section 3 briefly explains the FVM for the laser. Then, Section 4 describes the asteroid rotational dynamics and implemented control strategies, along with the semi-analytical equations used to integrate the deflection action for long period. Finally, Section 6 shows the results. In particular Section 6.1 identify when the orbit is relatively clear of debris for different scenarios, while Section 6.2 compares the different deflection strategies for different operational altitude.

## **2. Particles dynamics**

It is assumed that the asteroid body frame is coincident with this frame at the beginning of the simulations.

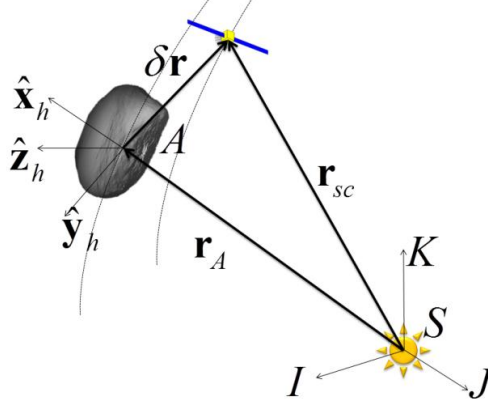


**Figure 1. Reference Frame.**

The debris is subjected to the force due to the gravity of the Sun, solar pressure and the irregular gravity of the asteroid. The nonlinear relative equations of motion are given by ([8]):

$$\delta\ddot{\mathbf{r}} + 2\boldsymbol{\omega}\dot{\mathbf{r}} + \boldsymbol{\omega}\times(\boldsymbol{\omega}\times\mathbf{r}) = -\frac{\mu_a}{\delta r^3}\delta\mathbf{r} + \mu_{Sun}\left(\frac{\mathbf{r}_a}{r_a^3} - \frac{\mathbf{r}_{sc}}{r_{sc}^3}\right) + \frac{\partial U_s}{\partial(\delta\mathbf{r})} + \mathbf{SRP}(\mathbf{r}_{sc}) \quad (1)$$

with  $\mu_{Sun}$  is the Sun gravity constant,  $\mu_a$  is the gravity constant of the asteroid,  $r_a$  and  $r_{sc}$  are the positions of the asteroid and debris with respect to the sun.  $\delta r$  is the relative distance between the debris and the asteroid.  $\boldsymbol{\omega}$  represents the instantaneous angular velocity with which the asteroid (i.e. the reference frame) rotates around the Sun.  $\mathbf{SRP}(\mathbf{r}_{sc})$  is the solar radiation pressure which depends on the distance from the Sun (as well as area, reflectivity coefficient and mass). The gravity field of the asteroid is given by the actual shape of the asteroid.  $U_s$  is the higher order potential of the asteroid. The derivation of the non-uniform gravity field  $U$ , comprehensive of the  $U_s$  and the uniform field giving origin to first contribution of Eq.(1), will be given in Section 2.1..

Beyond the gravitational perturbations from the asteroids, the major perturbation is the solar radiation pressure  $\mathbf{SRP}(\mathbf{r}_{sc})$ .

$$\mathbf{SRP}(\mathbf{r}_{sc}) = C_r S_{srp} \left(\frac{r_{1AU}}{r_{sc}}\right)^2 \frac{r_{sc}}{r_{sc}} \frac{A}{m_{sc}} \quad (2)$$

$A$  and  $m_{sc}$  are the debris cross section area and mass, respectively,  $C_r$  is the reflectivity coefficient and  $S_{srp}$  is the solar radiation pressure at 1 AU,  $r_{1AU}$  is equivalent the astronomical unit in km. The motion of the asteroid with respect to the Sun is given as:

$$\delta\ddot{\mathbf{r}}_a = -\frac{\mu_{Sun}}{r_a^3}\mathbf{r}_a \quad (3)$$

## 2.1. Shape gravity field

The gravity model works for an arbitrary shape and was implemented from the equations used in [9]. This model assumes a uniform density of the asteroid and allows expressing the local acceleration in an arbitrary location of space with respect to the asteroid's centre of mass. It is

especially suited for proximity operations, where the harmonic techniques fail to provide an accurate representation of the gravity field.

With reference to Figure 2, the local acceleration is given by the gradient of the potential field U by

$$\nabla U = -G\rho \sum_{e \in \text{edges}} L_e \tilde{\mathbf{E}}_e \mathbf{r}_e + G\rho \sum_{f \in \text{faces}} \omega_f \tilde{\mathbf{F}}_f \mathbf{r}_f \quad (1)$$

where  $\vec{r}_e$  is the distance of a generic point from the edge, and  $\vec{r}_f$  is the distance from the centre of the facet.  $\tilde{\mathbf{E}}_e$  and  $\tilde{\mathbf{F}}_f$ , respectively the edge and the facet dyads in this expression, are computed on each triangular face with reference to Figure 2 as follows:

$$\begin{aligned} \tilde{\mathbf{E}}_e &= \mathbf{n}_A \mathbf{n}_{21}^A + \mathbf{n}_B \mathbf{n}_{12}^B \\ \tilde{\mathbf{F}}_f &= \mathbf{n}_f \mathbf{n}_f \end{aligned} \quad (2)$$

The edge dyads use the normals to faces and edges,  $\vec{n}_f$  and  $\vec{n}_{ij}^f$  of two adjacent faces. The normals to faces and edges are calculated from the coordinates of the vertices as:

$$\begin{aligned} \mathbf{n}_f &= (\mathbf{r}_2 - \mathbf{r}_1) \times (\mathbf{r}_3 - \mathbf{r}_2) \\ \mathbf{n}_{ij}^f &= (\mathbf{r}_j - \mathbf{r}_i) \times \mathbf{n}_f \end{aligned} \quad (3)$$

Dimensionless factors  $L_e$  and  $\omega_f$  are then given by

$$\begin{aligned} L_e &= \ln \frac{r_i + r_j + e_{ij}}{r_i + r_j - e_{ij}} \\ \omega_f &= 2 \tan^{-1} \frac{r_i r_j \times r_k}{r_i r_j r_j + r_i (r_j r_k) + r_j (r_i r_k) + r_k (r_j r_i)} \end{aligned} \quad (4)$$

where  $e_{ij}$  is the length of the edge.

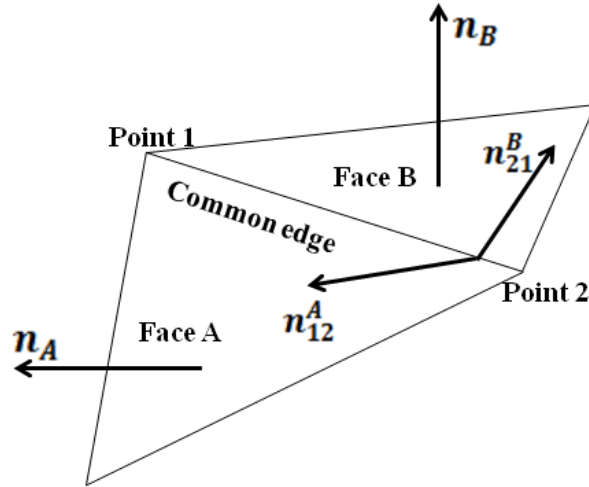


**Figure 2. Reference directions and notations for the shape model equations.**

Figure 3 shows for example the resulting accelerations on the surface of asteroid (433) Eros, computed by using our script on the barycentre of each triangle faces.

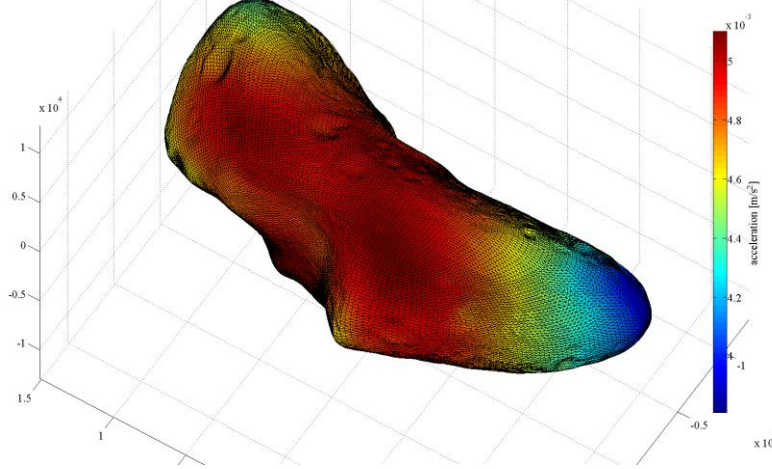


**Figure 3. Local acceleration on the surface of asteroid (433) Eros.**

## 2.2. Initial particle conditions

The initial velocity was generated considering two vectorial components:

$$v_{\text{debris}} = v_t + v_1 n \quad (4)$$

- The first was given by the tangential component given by the rotation of the asteroid around c-axis

$$v_t = \Omega \wedge r_s \quad (5)$$

Where  $r_s$  is the initial position the surface of the asteroid and  $\Omega$  is the angular velocity of the astroid around  $z_h$ -axis .

- The second component was given considering a fraction of excess velocity which allows inserting the debris into an escape trajectory ([10]).

$$v_1 = k \left( -n \cdot v_t + \sqrt{(-n \cdot v_t)^2 + 2U_{\text{kep}} - v_t^2} \right) \quad (6)$$

where  $k$  represent the fraction of excess velocity considered (between 0 and 1),  $n$  is the normal to the surface,  $U_{\text{kep}}$  is the 2-body gravity potential at  $r_s$ .

In order to generate samples departing into different directions the second component was rotated around the normal direction with angles from  $-\frac{\pi}{2}$  to  $\frac{\pi}{2}$ . The propagation stopped in the case of impacts on the surface of the asteroid. The particle was considered to leave the orbit of the asteroid when its Keplerian energy was positive (equivalently to having eccentricity higher than 0).

## 3. Laser Model

The following section briefly introduces the finite volume module simplification which was used for calculating the imparted thrust. The interested reader could refer [7] in order to acquire more information and details about this derivation. The laser-matter interaction model aims at computing the momentum imparted to the asteroid in function of its physical and dynamical properties as well as the key parameters of the laser system, namely the output power and the focusing capabilities. Namely, the figure of merit is given by the momentum coupling coefficient, representing the amount of thrust one gets per optical watt of power invested in the process:

$$C_m = \frac{T}{P} \quad (5)$$

With reference to Figure 4 the coupling coefficient is recovered after solving the transient 1D equation in presence of vaporization and melting:

$$\frac{\partial H}{\partial t} = -\frac{\partial q}{\partial z} + u \frac{\partial H}{\partial z} \quad (6)$$

In this expression,  $H$  represents the enthalpy of the material per unit volume,  $u$  the recession speed of the interface and  $q$ , the heat flux.

The domain was discretized in  $N$  discrete volumes over which the enthalpy conservation holds:

$$\frac{dH_i}{dt} = -\frac{q_{i+1/2} - q_{i-1/2}}{\Delta z} + u \frac{H_{i+1} - H_i}{\Delta z} \quad (7)$$

The boundary conditions were set as following:

- Vaporization:  $q_{1/2} = \alpha_M \Phi - \rho u E_v$
- Last cell:  $q_{N+1/2} = -k \frac{T_\infty - T_N}{\Delta z}$

where  $\Phi$  is the laser flux. The heat fluxes themselves are computed from the discretized Fourier law:

$$\bullet \quad q_{i-1/2} = -k \frac{T_i - T_{i-1}}{\Delta z} \quad (8)$$

$$\bullet \quad q_{i+1/2} = -k \frac{T_{i+1} - T_i}{\Delta z} \quad (9)$$

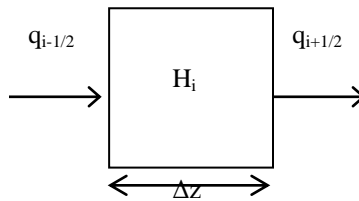


**Figure 4. Elementary surface geometry.**

The enthalpy formulation allows accounting for the presence of a moving melting front within the substrate and is for convenience defined to 0 at the melting point. The temperature is recovered at each time-step from the enthalpy:

- Liquid ( $H_i > \rho E_m$ ) :  $T_i = T_m + \frac{H_i - \rho E_m}{\rho c_l}$
- Transition ( $\rho E_m > H_i > 0$ ) :  $T_i = T_m$
- Solid ( $0 > H_i$ ) :  $T_i = T_m + \frac{H_i}{\rho c_s}$

The recession speed depends on interface temperature only:  $u=u(T_i)$ . The dependency was obtained by strictly following the methodology proposed by Knight [4] and considering a sonic ejection speed in vacuum. This leads to an expression formally similar to the well-known Hertz-Knudsen-Langmuir formula. During the time-integration, the pressure  $p_e$  and velocity  $v_e$  in the gas on the edge of the Knudsen layer are reconstructed from the surface temperature, allowing computing the real-time evolution of the momentum coupling coefficient which is the ratio between the effective pressure and the flux  $\Phi$ :

$$C_m(t) = \frac{T}{p} = \frac{p_e + \rho_e v_e^2}{\Phi} = \frac{(\gamma+1)p_e}{\Phi} \quad (10)$$

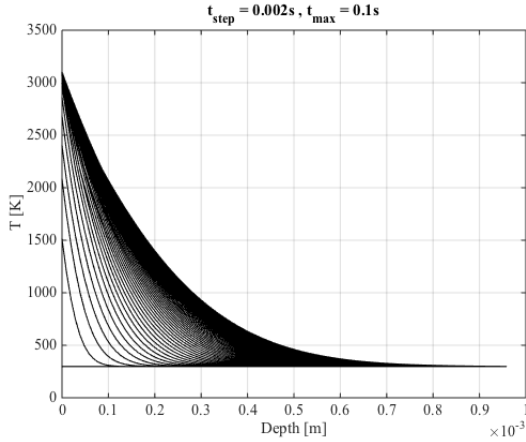


**Figure 5: Evolution of the temperature beneath the spot for a flux of  $100\text{W}/\text{mm}^2$ .**

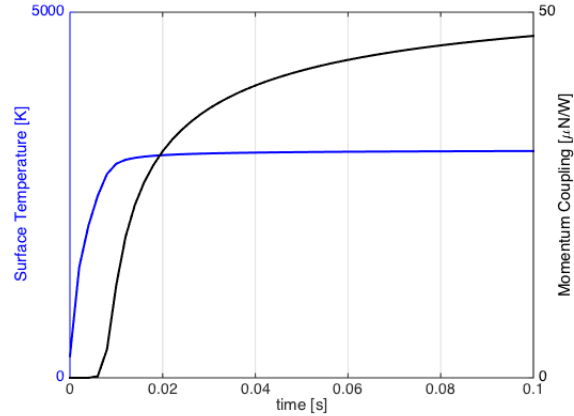


**Figure 6: Evolution of the Momentum Coupling and Surface Temperature for a flux of  $100\text{W}/\text{mm}^2$ .**

Figure 5 and Figure 6 show the evolution of the temperature distribution, momentum coupling and surface temperature respectively, for a flux on the target of  $100\text{W}/\text{mm}^2$ .

The average amount of time  $\tau$  during which a given point on the surface of the asteroid remains heated by the laser beam is function of the local velocity of the asteroid surface and the beam diameter  $\phi$ :

$$\tau = \frac{\pi\phi}{4v_{loc}^{\perp}} \quad (11)$$

The effective momentum coupling is obtained by averaging its value over the heating time.

$$C_m^{eff} = \frac{\eta}{\tau} \int_0^{\tau} \frac{(\gamma+1)p_e}{\Phi} dt \quad (12)$$

In this expression,  $\eta$  is a geometrical efficiency which depends on the non-dimensional ratio

$$\xi = \alpha_M c_l \Phi \phi / k \quad (13)$$

The factor  $\eta$  represents the losses due to lateral conduction and non-ideal beam quality and was obtained by fitting the results of the present model to a 3D FEM model for different values of the  $\xi$  parameter as:

$$\eta = \frac{0.87}{1 + (1.625 \xi)^{-1}} \quad (14)$$

The momentum coupling computed by the model is represented in Figure 7 in function of the laser system parameters and assuming a local surface speed of 10 cm/s.

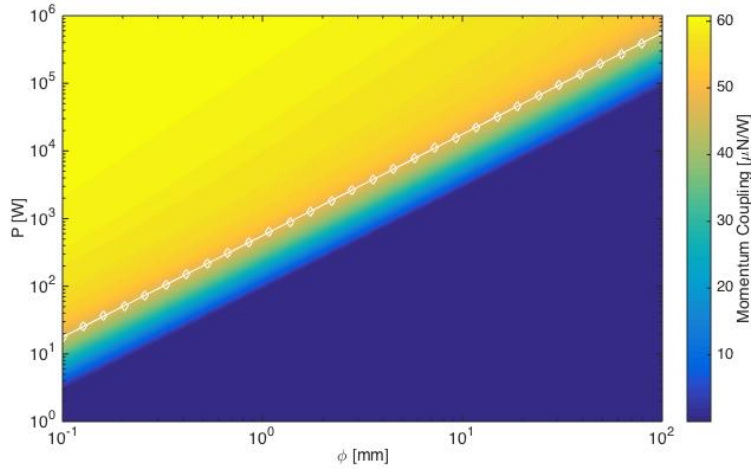


**Figure 7: Momentum coupling in function of the focusing and optical power.**

An empirical requirement was also found to ensure a minimum coupling of 40  $\mu\text{N/W}$ :

$$\Phi \sqrt{\frac{\tau}{10}} > 20W / \text{mm}^2$$

This critical requirement is represented by the white line in Figure 7. The variation of the deflection time with the defocusing of the beam is however a function of the rotation rate. A variation of the distance will produce a bigger cross section  $A_{spot}$  of radius  $w$  on the surface of the asteroid consistently with the Rayleigh length, as shown in the following equation:

$$\begin{aligned} w(l) &= w_0 \sqrt{1 + \frac{|l - l_{focusing}|}{l_{Rayleigh}}} \\ A_{spot} &= \pi w^2 = \pi w_0^2 \left( 1 + \frac{|l - l_{focusing}|}{l_{Rayleigh}} \right) \end{aligned} \quad (15)$$

where  $l$  is the distance from the spot,  $l_{focusing}$  is the focusing length. This means that the light intensity at the spot decreases as the distance of the laser source from the surface departs from the focusing distance. Nonetheless, it was assumed that the laser system is able to adjust its focussing with respect to the distance between the spacecraft and the impinging spot. The reason for this is due to the fact that the Rayleigh length is generally in the order of few meters, while the distance between the spacecraft and the impinging spot could vary by tens of meters, preventing the ablation process.

If the incident laser beam is not perpendicular to the surface the spot deforms from a circle to an ellipse and its area increases. The travel time of a point under the spot light tout-tin then changes depending on the direction of the velocity  $V_{rot}$  with respect to the local normal and Eq.(2) needs to be modified to account of the actual geometry. Consistently with previous work of [5], a simpler and more conservative approach is taken. Instead of calculating the exact travelling time the light intensity is simply reduced by modifying Eq. (15) as follows:

$$A_{spot} = \pi w^2 = \pi w_0^2 \left(1 + \frac{|l-l_{focusing}|}{l_{Rayleigh}}\right) \frac{1}{\cos \theta_{laser-normal}} \quad (16)$$

where  $\theta_{laser-normal}$  is the angle between the incident laser beam and local normal. The area given by Eq. (16) is then used to calculate the current power flux. As one can see as the cross section increases with this angle, the power density decreases and progressively reduces to zero for nearly tangential configurations.

In order to fully understand the following results Figure 8 shows the nominal trend for the thrust level and the time to lose 50% of the available power due to the contamination affecting the solar array. Here we assumed to place the laser at 300 m, with 1 mm diameter of the laser beam. The time to lose 50% power was calculated assuming the power is maintained fixed during operations. As for the results of the analyses, we assumed that the solar arrays will be in the middle of the plume, which implies the maximum contamination levels during the whole period. Table 1 reports following characteristics for simulating the laser ablation processes:

**Table 1. Laser system coefficients and ablation parameters.**

Parameter	Value
$\tau_g$	1
$\alpha_M$	0.84
$\eta_p$	0.85
$\eta_L$	0.55
$\eta_s$	0.3
$\eta$	2·10 <sup>-4</sup> cm <sup>-1</sup>
$c_A$	1361 J/(K·kg)
$\kappa_A$	4.51 W/(m·K)
$\rho_A$	2500 kg/m <sup>3</sup>
$T_s$	3800 K

Figure 8 (left) shows the thrust trend for the FVM. It appears to be not much sensitive to the rotational velocity. Nonetheless as the power increases the efficiency of the laser is less sensitive to the rotation. The effect on the contamination is quite noticeable, as shown in Figure 8 (right). In fact FVM brings high level of thrust but at the same time the contamination levels result predominant at high laser power. This is something which will greatly affect the overall performance.

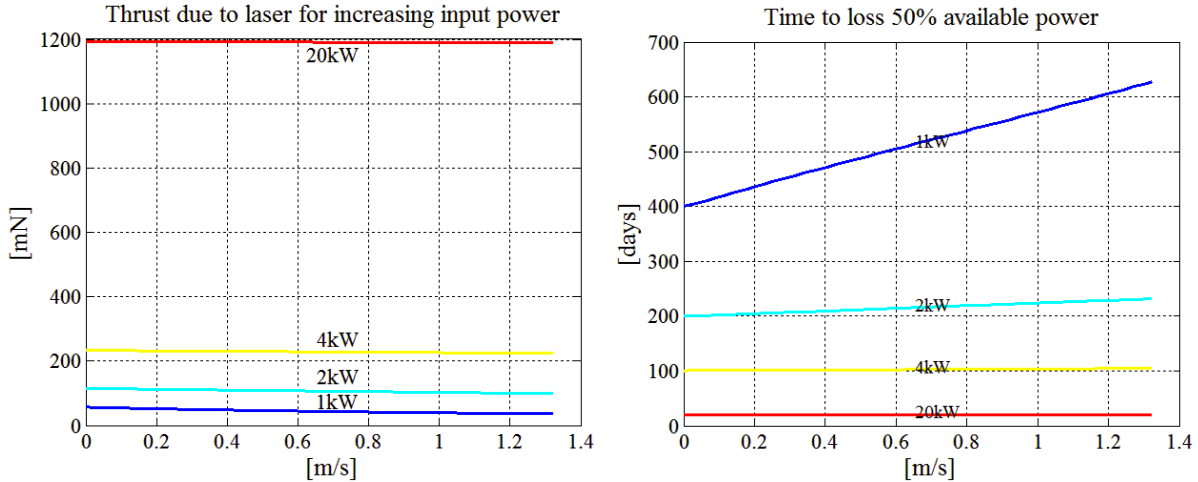


**Figure 8. Thrust trend with power for increasing surface velocity (left) and contamination rate trend with power for increasing surface velocity (right).**

#### 4. Asteroid orbit and rotational control

In principle controlling the rotational motion of the asteroid will lead to higher efficiency because reducing the angular velocity increases the power transfer from the laser to the surface in the unit of time. Nonetheless as the mass, and subsequently the inertia, of the spacecraft increases, this option is not always feasible in short operating period using limited power. For this reason besides the rotational control in Section 4.1, also pure orbit control was considered in Section 4.2.

##### 4.1. Pure asteroid Rotational Control

The ablation force is higher when the velocity  $V_{rot}$  is lower because the time interval  $[t_{in} t_{out}]$  to sublimate the surface tends to infinity. The velocity  $V_{rot}$  is given by the modulus of the cross product of the instantaneous angular velocity and  $\mathbf{s}$ , the position vector of the spot on the surface of the asteroid, with components  $\mathbf{s} = [s_x^b \ s_y^b \ s_z^b]^T$  in the body frame:

$$V_{rot} = \|\boldsymbol{\omega} \times \mathbf{s}\|$$

This means that decreasing the asteroid's angular velocity can increase the yield of the ablation process. The asteroid's rotational motion is governed by the following system of differential equations:

$$\begin{aligned} \dot{\mathbf{q}}^a &= \frac{1}{2} \mathbf{\Pi} \mathbf{q}^a \\ \mathbf{I} \dot{\boldsymbol{\omega}} + \boldsymbol{\omega} \mathbf{I} \boldsymbol{\omega} &= \mathbf{M}_c \end{aligned} \quad (17)$$

where  $\mathbf{q}^a = [q_1^a \ q_2^a \ q_3^a \ q_4^a]$  is the quaternions vector,  $\boldsymbol{\omega} = [\omega_x \ \omega_y \ \omega_z]$  is the angular velocity vector in the body frame,  $\mathbf{I}$  is the matrix of inertia of the asteroid,  $\mathbf{M}_c$  is the control torque, and  $\mathbf{\Pi}$  is given by:

$$\mathbf{\Pi} = \begin{bmatrix} 0 & \omega_z & -\omega_y & \omega_x \\ -\omega_z & 0 & \omega_x & \omega_y \\ \omega_y & -\omega_x & 0 & \omega_z \\ -\omega_x & -\omega_y & -\omega_z & 0 \end{bmatrix} \quad (18)$$

Perturbative torques from the Sun light pressure and the YORP effect are neglected because their cumulative effect is negligible with respect to the torque induced by the laser.

A strategy to reduce the spinning rate of the asteroid, which was investigated, was to apply a control torque proportional to the opposite of the angular velocity vector:

$$\mathbf{M}_c \propto -\boldsymbol{\omega} / \omega \quad (19)$$

The actual control torque  $\mathbf{M}_c$  that can be generated is given by the cross product of the thrust  $\mathbf{F}_L^b$  with the position vector  $\mathbf{s}$ .  $\mathbf{F}_L^b$  is the thrust vector, projected in body axes, produced by the ablation process at point  $\mathbf{s}$  on the surface of the asteroid (see Figure 9).

We know that the force exerted by the laser is perpendicular to the local normal. In this way knowing the shape of the object and, thus, the direction of the normals to its surface is sufficient for determining the direction of all the possible control torques. Following the results of [5], we point the laser with the following control logic

$$\min_s \mathbf{M}_c(\mathbf{s}) \cdot \boldsymbol{\omega} \quad (20)$$

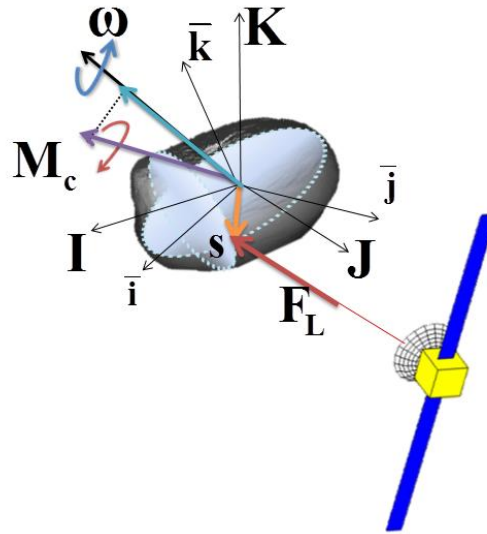
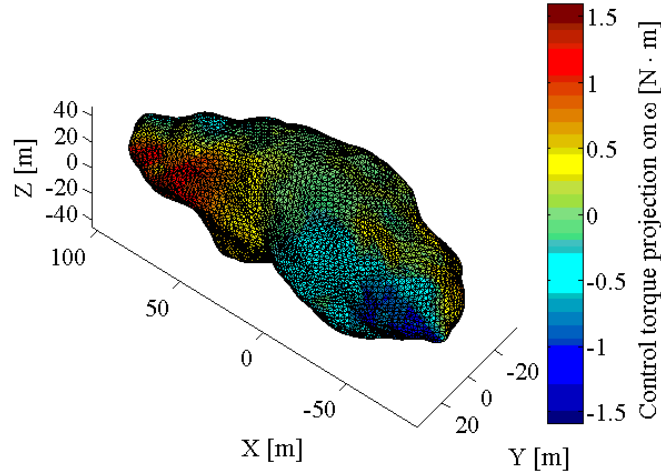


Figure 9: Angular velocity control scheme.

This means that the laser will hit the points on the surface of the object, where the misalignment of the control torque with respect to the angular velocity will be the minimum. An example of this approach can be seen in Figure 10 for an irregular body rotating clockwise around z-axis. The red spot produces a thrust, whose control torque is directed counter clockwise.



**Figure 10. Example of control torque distribution for a 100 m irregular shape asteroid and 1 kW laser.**

#### 4.2. Pure asteroid Orbit Control

Alternatively if one neglects the possibility to control the asteroid rotation, different pointing strategies could be used. Two strategies were explored:

- The laser will be pointed such that the resulting thrust will be as much as possible aligned with the desired deflective action (for example along the orbit tangential which maximize the overall displacement).

$$\min_s \mathbf{n}(s) \cdot \widehat{\mathbf{n}}_{desired} \quad (21)$$

where  $\mathbf{n}$  is the local normal – which gives the direction of the resulting thrust – and  $\widehat{\mathbf{n}}_{desired}$  is the desired normal. An example of this process can be seen in Figure 11 where the laser is placed along the y-axis.

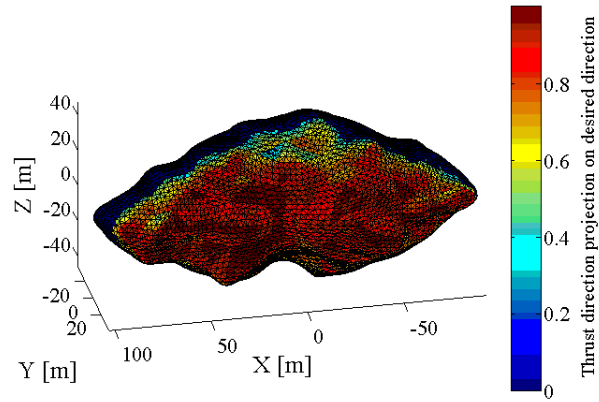


**Figure 11. Example of surface points producing thrust directed as the desired one.**

- The laser will be pointed fixed towards the asteroid. The intersection point is identified as the barycentre of the triangle of the asteroid mesh closest to spacecraft position vector  $r_{SC}$ . In practice:

$$\min_s \widehat{s \cdot r_{SC}} \quad (22)$$

An example of the implemented procedure is shown in Figure 12, where the red areas represent the closest points to the laser beam (the laser is placed along y-axis).

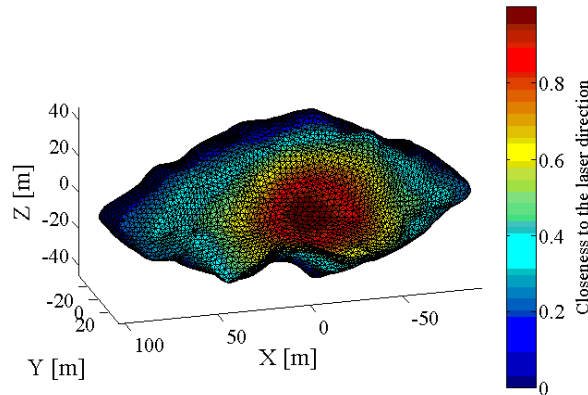


**Figure 12. Example of the identification of points closer to the laser beam direction.**

### 4.3. Long term Evolution

The effect on the displacement from its nominal position at a given point along the orbit depends on the direction of the thrust. Coupled orbit and rotational dynamics would require long computational time for long period simulations. For this reason a simpler approach was implemented. The different control schemes of Section 4.1. and Section 4.2. were simplified, calculating mean directions of thrust, along with mean angular velocity variation for different nominal powers and nominal angular velocities. The single value was calculated by considering the actual geometry of the asteroid over a control period of 7 days. It is true that the calculation

of these quantities is slightly affected by the initial attitude, but this effect is filtered out when averaging over considerable longer period than the body revolution period around its axes. In this way a variational approach can be faster implemented.

Let  $a$ ,  $e$ ,  $i$ ,  $\Omega_a$ ,  $\omega_a$  and  $M_a$  be respectively the semi-major axis, eccentricity, inclination, anomaly of the ascending node, anomaly of the pericentre and mean anomaly of the nominal orbit of the asteroid. The effect of the deflection is calculated at predefined check-points. Let  $t_{check}$  be the instant of time corresponding to a generic check point. If  $\vartheta_{check}$  is the true anomaly of the asteroid, and  $\vartheta_{check}^* = \vartheta_{check} + \omega_a$  the corresponding argument of latitude, one can write the variation of the position of the asteroid after deviation, with respect to its unperturbed position, by using the proximal motion equations as in [6] and [7]:

$$\delta \mathbf{r}_a(t_{check}) = \mathbf{A}_{check} \delta \boldsymbol{\alpha}(t_{check}) \quad (23)$$

where  $\delta \mathbf{r}_a = [\delta x_{h-a} \ \delta y_{h-a} \ \delta z_{h-a}]^T$  with  $\delta x_{h-a}$ ,  $\delta y_{h-a}$  and  $\delta z_{h-a}$  the displacements in the radial, transversal and out of-plane directions in the Hill's reference frame centred at the unperturbed position of the asteroid at the check point. The vector  $\delta \boldsymbol{\alpha}(t_{check}) = [a \ e \ i \ \Omega_a \ \omega_a \ M_a]$  is the variation of the orbital parameters at the check-point and the matrix  $\mathbf{A}_{check}$  transforms the variation of the orbital parameters in trajectory displacements. The assumption used to compute displacement is that the variation of the relative position  $\delta \mathbf{r}_a = \|\delta \mathbf{r}_a\|$  is small compared to the unperturbed orbit radius  $r_{check}$ , that is  $\delta \mathbf{r}_a \ll r_{check}$ .

## 5. Results

### 5.1. Asteroid's model

Let us describe first the asteroid's model and selection. As of June 14th, 2015 there are 12730 asteroids in the NEODyS database, of which 514 are Near-Earth asteroids (NEAs) present in the risk list<sup>1</sup>. Asteroids in the catalogue vary from few meters to tens of kilometres in diameter. We are interested in relatively small asteroids (few metres in diameter) belonging to the S-type. A suitable one is represented by 2013XK22 asteroid whose nominal trajectory is  $[a, e, i, \Omega_a, \omega_a] = [1.045AU \ 0.2034 \ 0.1221rad \ 3.1876rad \ 4.6374rad]$ . To estimate the size of an asteroid, given its orbital parameters and absolute magnitude  $H$  only, we use the well-known formula

$$D = \frac{1}{\sqrt{p_v}} 1329 [\text{km}] \times 10^{-H/5},$$

where  $p_v$  is the asteroid's albedo, which is assumed to be 0.154 for standard NEAs and 0.18 for S-type asteroids. Inverting the equation for the absolute magnitude, we have

$$H = -5 \log_{10} \frac{D \sqrt{p_v}}{1329 [\text{km}]}.$$

Thus, for  $D = 100$  m and  $0.154 \leq p_v \leq 0.18$ , we find  $H \approx 24$ . The angular velocity of the asteroid is given by

<sup>1</sup> <http://newton.dm.unipi.it/neodyS>

<sup>2</sup> [https://starbase.jpl.nasa.gov/ear-a-5-ddr-radarshape-models-v2.0/as2004\\_0001/data/rshape04/](https://starbase.jpl.nasa.gov/ear-a-5-ddr-radarshape-models-v2.0/as2004_0001/data/rshape04/)

$$\omega_{limit} = \sqrt{\frac{4}{3}\pi\rho\mu_A},$$

where  $\rho$  is the asteroid density and  $G$  the gravitational constant. The formula above gives the spin limit in the gravity regime that is the angular speed at which an object will start to defragment. Hence, it is crucial for objects held together by self-gravity. However, it has been shown that the spin limit formula holds for any objects larger of 200 m. Objects smaller than 200 m have been observed to rotate faster than the spin limit prediction. Anyway lacking of direct measurements we took this limit as reference rotational velocity for the study. It results that for a density of  $2500 \text{ kg/m}^3$  the angular velocity is about 170 deg/h.

In the following the mass of the asteroid is  $1.2919 \cdot 10^9 \text{ kg}$ , with the shape taken from the (1620) Geographos asteroid and scale down to the mean radius of 50 m. The actual max sizes along three body axes are [103.4 39.4 46.3] m. The resulting inertial matrix as calculated numerically is:

$$I = \begin{bmatrix} 0.7383 & 0.0032 & 0.0349 \\ 0.0032 & 2.6203 & 0.0111 \\ 0.0349 & 0.0111 & 2.5149 \end{bmatrix} \text{ kgkm}^2$$

The shape models were obtained from the NASA Planetary Data System<sup>2</sup>. Figure 13 illustrates such a triangular shape model for the asteroid (1620) Geographos.

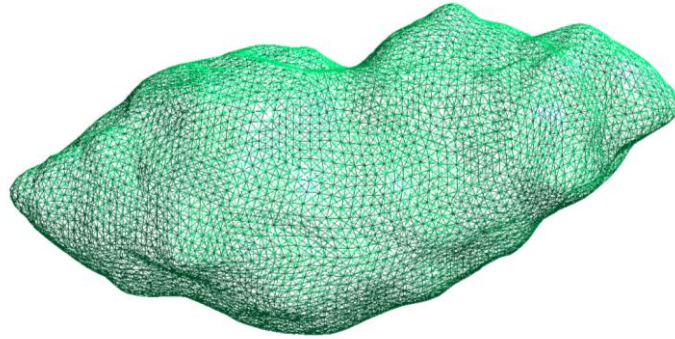


**Figure 13. Mesh of the asteroid (1620) Geographos.**

From such a model, the inertia tensor of the complete asteroid was computed by dividing its volume in elementary elongated tetrahedra formed by adding the CoG of the asteroid to the surface triangles. The inertia matrix of the single tetrahedron was then computed using the formula developed by [9], using the CoG as the reference point. From this, the global inertia tensor is simply computed by summing the different elementary inertia tensors.

As a concluding note, the selected trajectory will not impact the Earth. For this reason we will simply compare the results to the nominal trajectory at the time of deflection, when considering the different strategies and time available to deflect in Section 5.2. and Section 5.3..

## 5.2. Debris from impactor

A number of test cases with the following parameters were considered:

<sup>2</sup>[https://starbase.jpl.nasa.gov/ear-a-5-ddr-radarshape-models-v2.0/as2004\\_0001/data/rshape04/](https://starbase.jpl.nasa.gov/ear-a-5-ddr-radarshape-models-v2.0/as2004_0001/data/rshape04/)

- Mean asteroid radius  $R_{obj} = 50$  m
- We considered  $1/k_{\omega}$  fractions of the angular velocity ( $[1/10 \ 1/4 \ 1/2 \ 3/4 \ 1]$ )
- Different value of are to mass ratio ( $[0.01, 0.005, 0.001]$ ) with a reflectivity coefficient of 1.3 (comprehensive of reflection and diffraction).

For each value of rotational velocity and A/m ratio, a number of initial conditions (circa 100,000 samples) was generated on the surface of the asteroid, at different location and different velocity. Then the orbits were propagated up to 1 year starting from perigee. For convenience we will present the results after one month, because the gravity field is so weak that after 2 months the area is completely clean of debris. We are interested in finding when it will be safe to start operations with the laser from the time the impactor has hit the surface.

Figure 15 shows synthetically the survival rate at the end of one orbital period for the previous analyses.

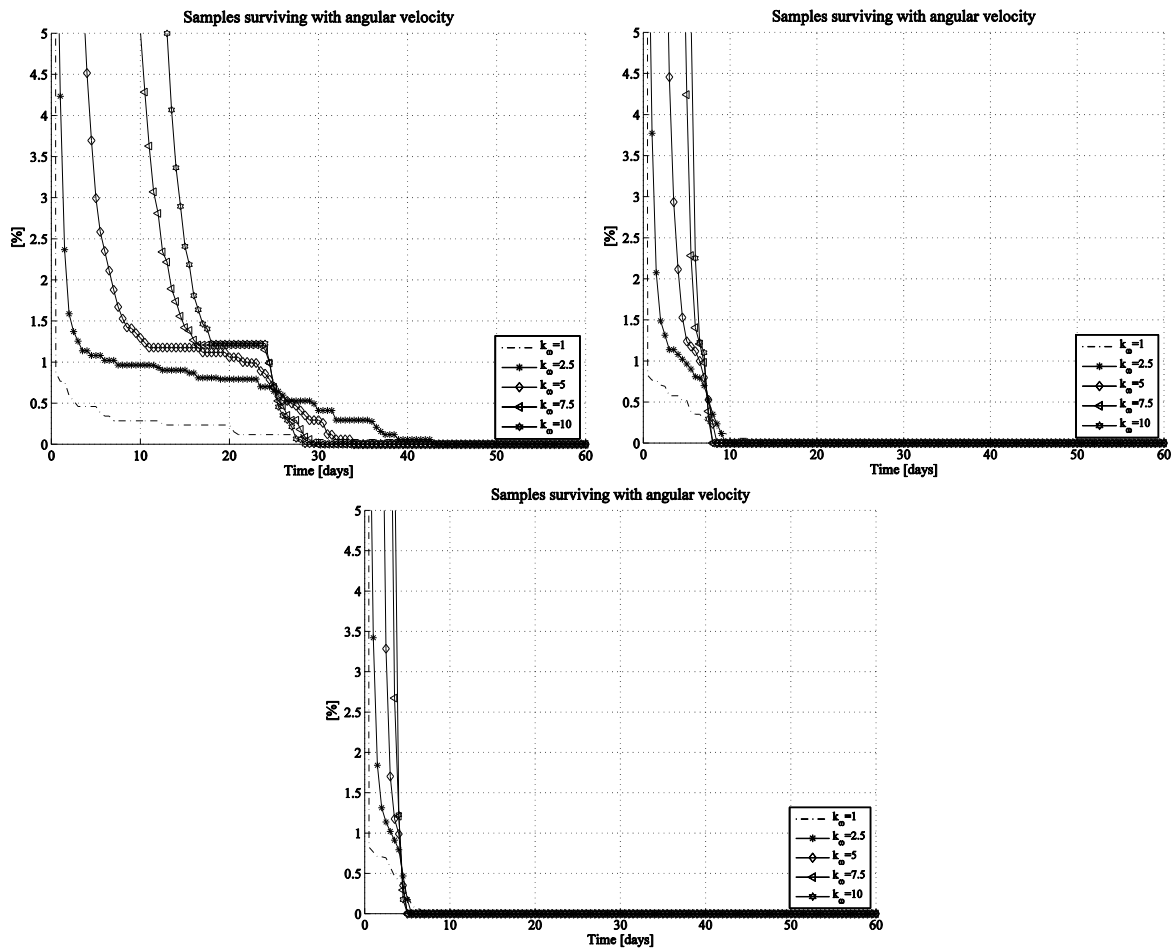


**Figure 14.** Number of surviving particles (left)  $A/m = 0.001 \text{ kg/m}^2$ , (right)  $A/m = 0.005 \text{ kg/m}^2$  and (bottom down)  $A/m = 0.01 \text{ kg/m}^2$ .

Few conclusions can be drawn:

- 1) The initial conditions plays important role in the number of surviving particles; if all the SRP is the same, particles with lower initial tangential velocity (due to the higher distance from the asteroid's centre of mass) will have more probability to survive for

longer period. Anyway the behaviour is not fully linear with time, given that for  $k_0=2.5$  more particles persist for longer.

- 2) The SRP will affect the survivability - in fact  $A/m = 0.001 \text{ kg/m}^2$  produces more surviving samples because particles are more affected by the asteroid's gravity and less by the SRP.

Although point 2) is not surprising, point 1) differs from the results of [4] where the trend was completely the opposite. An explanation can be found in the fact that this asteroid is 2 order of magnitude smaller, thus at the beginning the particles with higher energy (close to 0) will experience SRP a gravity and will escape more easily the asteroid. It is shown that more than 99.5% are no longer in the proximity of the asteroid after 30 days. Note that the area which can be considered safe is above the Hill's radius that is above circa 16 km for this asteroid. Anyway only handful debris particles are still in orbit, and none of them will be in orbit after 2 months from the impact.

### **5.3. Deflection**

In the following we want to identify suitable operational distance from which the spacecraft arrays will be less likely to downgrade. Of course moving very far from the surface will result in negligible contamination levels, but controlling the laser focusing farther from the asteroid will be challenging for the optics and possibly navigation system. For this reason we limited the maximum distance to 300 m. Figure 15 shows the ideal deflection case where the thrust is totally aligned with the orbital tangent. The trends are very similar to the previous case, with the total deflection scaled down for the effect of the contamination. When the laser is at 100 m, the contamination levels are so high that the achieved deflection is less than half an Earth radius. At 200 m more than 1 Earth radius deflection can be obtained in 20 years when the available power is above 4 kW. At 300 m such a deflection is achieved with 1.5 kW laser. The minimum time required is about 8 years with a 20 kW laser.

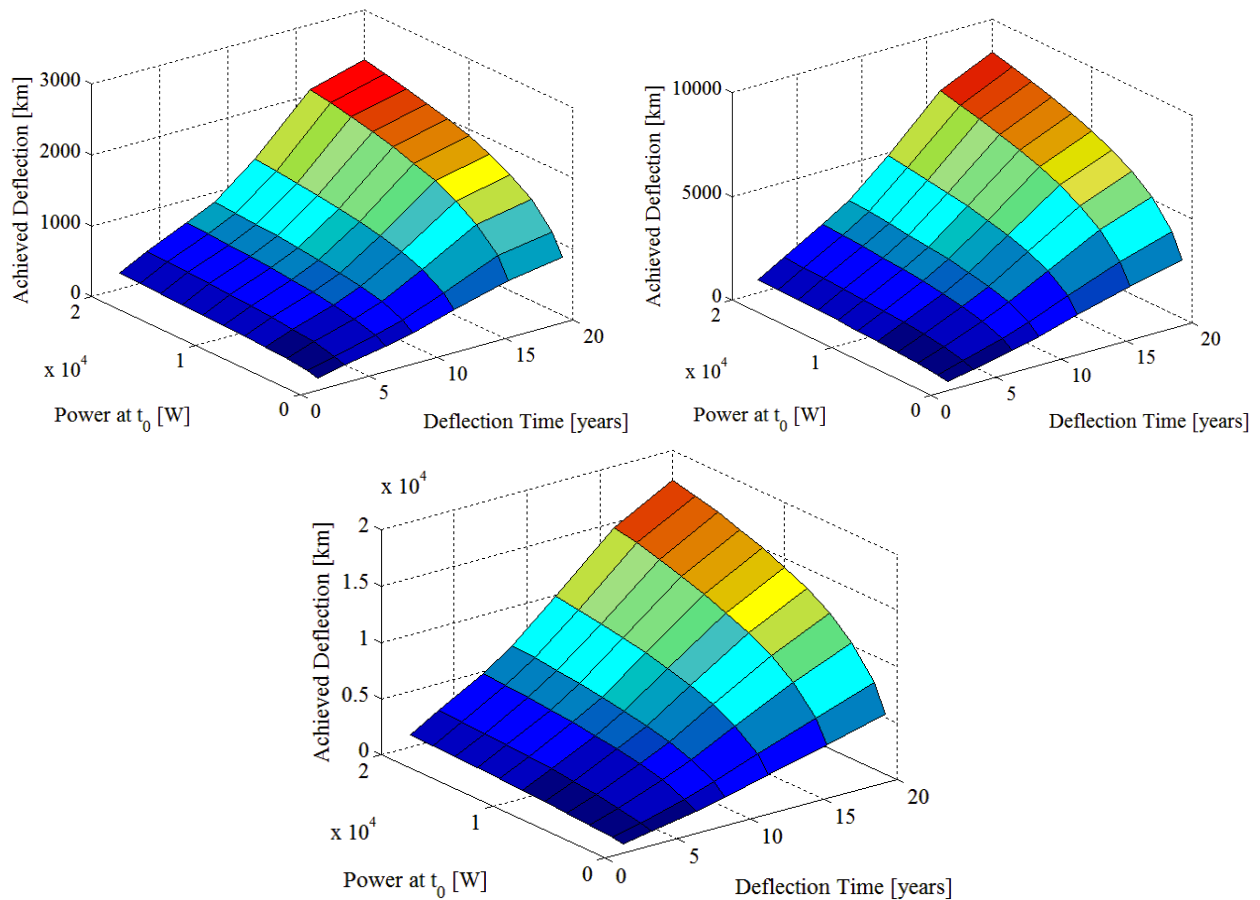


**Figure 15. FVM ideal deflection with spacecraft at 100 m (left), 200 m (right) and 300 m (bottom down).**

### 5.3.1. Angular control

As made with the previous laser model, we report the evolution of the angular velocity during 20 years operations in Figure 16. Also in this case the laser is placed at 300 m as an example. Basically no rotational control can be exerted on the asteroid, due to the big inertia matrix, high asteroid velocity and contamination which affect the thrusting process.

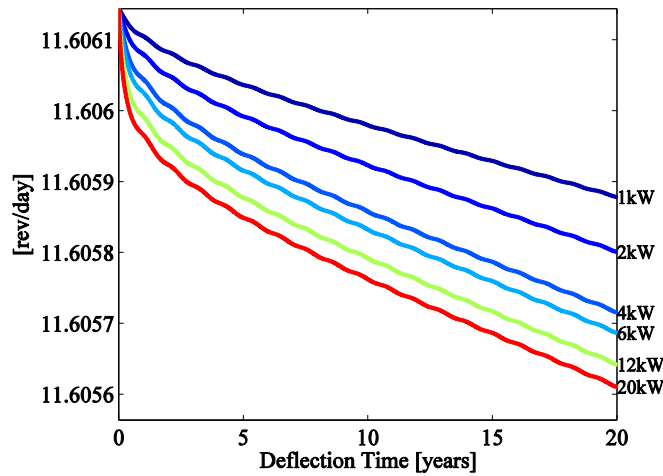


**Figure 16. Angular control over 20 year period for increasing powers at the laser – spacecraft at 300 m.**

For this reason the asteroid control does not produce high deflections. Figure 17 shows the achieved deflection as a function of time and power available placing the laser at 200 m and 300 m. As with the previous model, the effect of the distance plays an important role, since the lower contamination levels yields to double the achieved deflection (from 7000 km to about 14000 km). The minimum time to achieve one Earth radius deflection is circa 11 years.

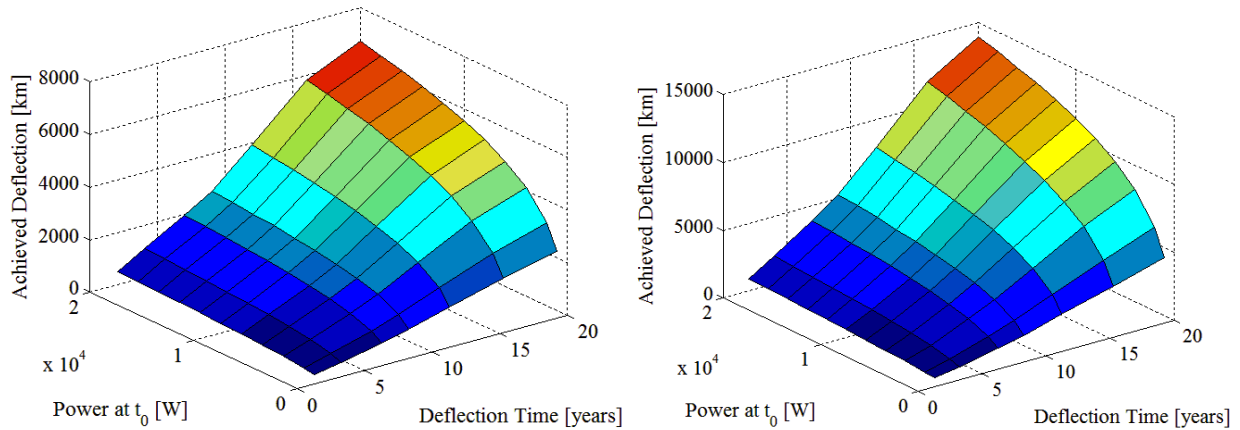


**Figure 17. Achieved deflection pursuing asteroid rotational control– laser at 200 m (left) and 300 m (right).**

The trend is similar to the one reported in Figure 15, but the effect of the shape and of the control strategy is such that the efficiency reduces by more than 20%.

### 5.3.2. Orbit control – optimising the direction of the thrust

The directional control on the resulting thrust will give substantial benefits with an overall efficiency of nearly 100% as shown in Figure 18 (with respect to the pure tangential case of Figure 17).

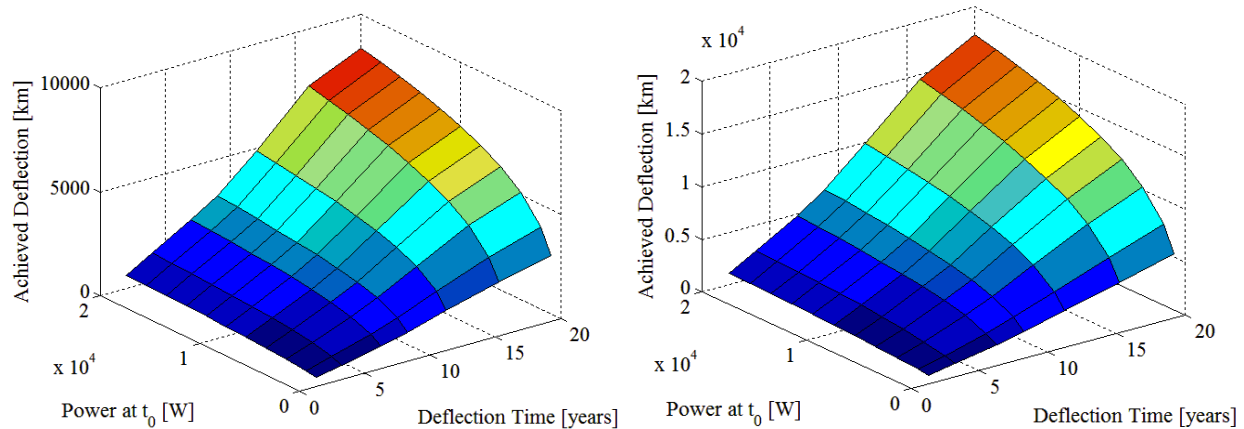


**Figure 18. Achieved deflection optimising the direction of the thrust – laser at 200 m (left) and 300 m (right).**

With respect to the rotational motion control, one Earth radius deflection can be achieved after 9 years, reducing the required time by 2 years if the laser is at 300 m from the target.

### 5.3.3. Orbit Control – maintaining fixed laser pointing

As for the previous laser model, the laser beam is pointed along the spacecraft-asteroid direction which coincides with the orbital tangent. Figure 19 shows the achieved deflection using this technique. As in the previous case the reduction with respect to the nominal case is by approximately 10%.

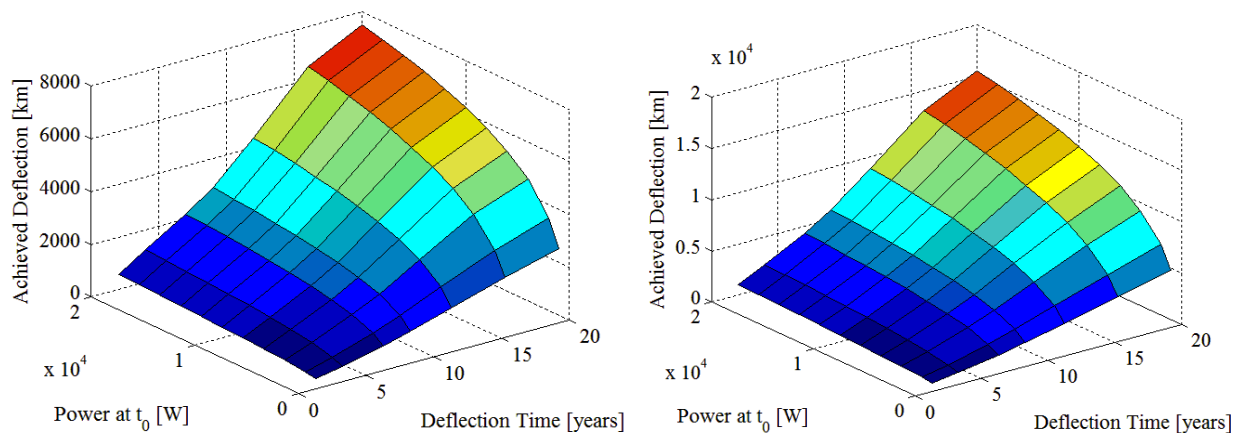


**Figure 19. Deflection obtained by pointing the laser along the spacecraft-asteroid direction– laser at 200 m (left) and 300 m (right).**

With respect to the thrust direction control, it takes an additional year to deflect the asteroid by one Earth radius.

### 5.3.4. Remarks

Figure 20 shows the time required to achieve one Earth radius  $R_{\text{Earth}}$  deflection comparing the analysed control methods for spacecraft placed at 200 m (left) and 300 m (right). We reported also the nominal deflection it would be obtained if the thrust was always tangential and the body was a sphere of 50 m diameter. The reader is reminded that the power at laser refers to 1 AU and initial time. It is clear that the rotational control perform poor compared to the other methods, because the thrust direction is continuously varied in opposite direction thus cancelling out the overall mean effect. This is more apparent when the spacecraft is at 200 m (Figure 20 - left); in that case the deflection is possible with more than 16 kW and 18 years continuous operation. On the contrary the thrust direction control produces more than 99% efficiency with respect to the nominal case, permitting to deflect the asteroid in 20 years by using about 8 kW. If the time concerns then 20 kW will reduce the deflection time to 14.5 years. In the case of the fixed pointing the minimum power to deflect the asteroid in 20 years is about 12 kW, while the minimum time is about 16 years with 20 kW. Moving at 300 m (Figure 20 - right), the overall performance is improved. Even a 2 kW is able to achieve this goal in less than 20 years for the thrust and fixed pointing control strategies. The rotational one requires about 4 kW. The minimum time with 20 kW was about 8.7 years for the thrust control, 9.5 years for the fixed pointing and 10.2 years for the rotational control.

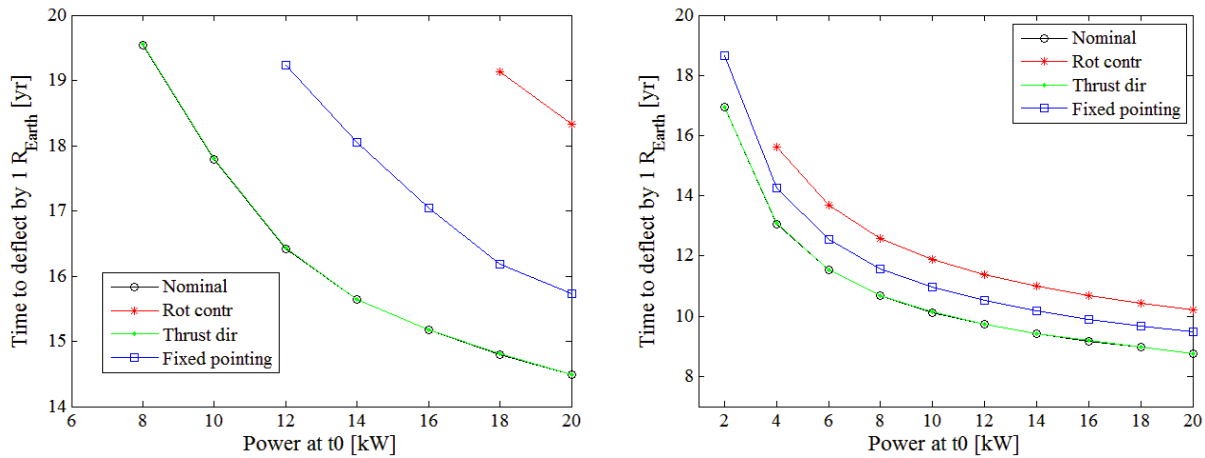


**Figure 20. Comparison between different control strategies: time to achieve 1  $R_{\text{Earth}}$  deflection - laser at 200 m (left) and 300 m (right).**

## 6. Conclusions

This paper presented an advancement of the available models for the problem of asteroid deflection by means of laser ablation. In particular a new finite volume model which takes into account the fact that the process of sublimation entails also a heat diffusive process under the surface. A simplified model which proved to agree with more complex 3D model has been used for simulating the deflective action. Moreover an accurate surface model which uses available shape data from actual asteroid was used for the laser analysis.

We first analysed the time a slow push deflection mission should start in the case a precursor impactor mission was carried out. The weak gravity field means that a possible impactor will produce a cloud of debris which will mainly soon flee the asteroid, while the remaining debris will orbit the asteroid for relatively short time. We saw that for a 100 m asteroid the orbit will be

clean by 99.5% debris after 30 days. This kind of analysis is size and shape dependant. In fact if the asteroid's size was bigger the debris will likely orbit the asteroid for more time.

When considering the laser ablation process, the resulting thrust depends on the local surface velocity and on normal to surface. We saw that the distance at which the spacecraft (and consequently the laser) is placed plays a fundamental role, because of the contamination levels. The study also analysed three different orbital control techniques for a 50 m diameter asteroid. The first aimed at reducing the angular velocity, in order to increase the thrust magnitude. The second and third techniques neglect the angular control. In particular the second tried to direct the thrust as the tangential direction which is the most efficient in terms of overall deflection, while the third maintains the direction of the laser beam fixed. The latter was actually conceived to be the simplest one from the operative point of view. We tested these techniques for different nominal powers and duration of operations. As expected the second technique results being the most efficient in terms of achieved deflection, while the fixed direction follows as second. The first option fails to bring substantial advantages, because no meaningful angular variations can be obtained with power limited to 20 kW. From these analyses the rotational control should be discarded as an option. On the contrary the thrust control will give the highest possible results, although it will require precise on-board capabilities to map the surface and correctly point and focus the laser in real time. The fixed pointing will require only adjusting the laser focusing as the surface move beneath.

With the constraints we set, deflecting the asteroid by one Earth radius will require 20 kW at the beginning of the mission (1AU) and about 9 year operations if we look at the fastest option. On the contrary if the time does not concern, the deflection can be achieved in 20 years with 2 kW. Anyway this option will likely require a number of spare spacecraft to perform such a mission. Finally we want to remark that the power was limited for practical reasons. If no limit is imposed, one can build similar analysis to identify the necessary power at the beginning of the operations able to guarantee one Earth's radius deflection in the available mission time.

## 6. References

- [1] Chapman C. R. and Morrison D., 1994. "Impacts on the Earth by Asteroids and Comets: Assessing the Hazard", *Nature*, Vol. 367, No. 6458, Jan. 1994, pp. 33–40, doi: 10.1038/367033a0.
- [2] Cheng, F.C. et al "AIDA: ASTEROID IMPACT & DEFLECTION ASSESSMENT". 64th International Astronautical Congress, Beijing, China. IAC-13-A3.4.8., 2013.
- [3] Sanchez J. P., Colombo C., Vasile M. and Radice G.: 2009, 'Multi-Criteria Comparison among Several Mitigation Strategies for Dangerous Near Earth Objects', *Journal of Guidance, Control and Dynamics*, Vol. 32, No. 1, Jan.-Feb. 2009, pp. 121-142, doi: 10.2514/1.36774.
- [4] Vetrivano, M., Puccacco, G., Celletti, A. "Asteroid debris: Temporary captures and escape orbits". To be submitted to *International Journal of Applied Mechanics and Engineering*, October, 2015.
- [5] Vasile M., Vetrivano M., Gibbings A., Garcia Yarnoz D., Sanchez Cuartielles J-P., Burns D., Hopkins J-M., Colombo C., Branco J., Wayman A., Eckersley S. "Light Touch2, Effective

- Solutions to Asteroid Manipulation“. ESA Final report, SysNova Study, ESA Reference Nos.: 12/X02, 12/X03, February 2013.
- [6] Vetrivano, M., Colombo, C. and Vasile, M. “Asteroid rotation and orbit control via laser ablation“. *Advances in Space Research*. Volume 56, Issue 8, Pages 1547-1804 (15 October 2015). doi:10.1016/j.asr.2015.06.035.
- [7] Thiry, N. and Vasile, M. “Recent advances in laser ablation modelling for asteroid deflection methods“. *Proceedings of SPIE - The International Society for Optical Engineering: Nanophotonics, Macrophotonics for Space Environments VIII*. Taylor, E. W. & Cardimona, D. A. (eds.). San Diego, California, Vol. 9226, 922608, 17 Sep 2014.
- [8] Scheeres, D. J., 2011. “Orbital Motion in Strongly perturbed Environments. Applications to Asteroid, Comet and Planetary Orbiters“. 1st edition, Springer-Praxis books in astronautical engineering. 2011.
- [9] Winkler, T., Kaplinger, B., & Wie, B. “Optical Navigation and Fuel-Efficient Orbit Control Around an Irregular-Shaped Asteroid“. *AIAA Guidance, Navigation, and Control (GNC) Conference*; 08/2013.
- [10] D. J. Scheeres et al. “Orbits Close to Asteroid 4769 Castalia“. *ICARUS* 121, 67–87 (1996). ARTICLE NO. 0072.
- [11] Knight, C. J. “Theoretical modeling of rapid surface vaporization with back pressure“. *AIAA journal*, 17(5), 519-523, 1979.
- [12] Vasile M., Colombo C. “Optimal Impact Strategies for Asteroid Deflection“. *Journal of Guidance, Control, and Dynamics*, Vol. 31, No. 4, July–August 2008, pp. 858–872, doi: 10.2514/1.33432.
- [13] Colombo C., Vasile M. and Radice G. “Semi-Analytical Solution for the Optimal Low-Thrust Deflection of Near Earth Objects“, *Journal of Guidance, Control and Dynamics*, Vol. 32, No. 3, May–June 2009, pp. 796–809, doi: 10.2514/1.40363.
- [14] Tonon, F. “Explicit exact formulas for the 3-D tetrahedron inertia tensor in terms of its vertex coordinates“. *Journal of Mathematics and Statistics*, 1(1), 8-11 (2005).